RSC Advances

This is an *Accepted Manuscript*, which has been through the Royal Society of Chemistry peer review process and has been accepted for publication.

Accepted Manuscripts are published online shortly after acceptance, before technical editing, formatting and proof reading. Using this free service, authors can make their results available to the community, in citable form, before we publish the edited article. This *Accepted Manuscript* will be replaced by the edited, formatted and paginated article as soon as this is available.

You can find more information about *Accepted Manuscripts* in the Information for Authors.

Please note that technical editing may introduce minor changes to the text and/or graphics, which may alter content. The journal's standard Terms & Conditions and the Ethical guidelines still apply. In no event shall the Royal Society of Chemistry be held responsible for any errors or omissions in this *Accepted Manuscript* or any consequences arising from the use of any information it contains.

ROYAL SOCIETY OF CHEMISTRY

www.rsc.org/advances

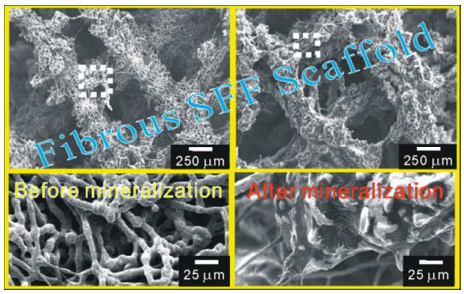

A 3D fibrous scaffold using an electrohydrodynamic jet process supplemented with *in vitro* mineralization to obtain a hydroxyapatite layer in simulated body fluid was fabricated.

RSC Advances Accepted Manuscript

Physical and biological activities of newly designed, macro-pore-structure-controlled 3D fibrous poly(ε-caprolactone)/hydroxyapatite composite scaffolds

Minseong Kim, MS and GeunHyung Kim, Ph.D*

Department of Bio-Mechatronic Engineering, College of Biotechnology and Bioengineering, Sungkyunkwan University, Suwon, South Korea. *E-mail: gkimbme@skku.edu; Tel: +82-31-290-7828; Fax: +82-31-290-7830.

Author address:

Minseong Kim, MS: Department of Bio-Mechatronic Engineering, College of Biotechnology and Bioengineering, Sungkyunkwan University, Suwon, South Korea. E-mail: hshomuboy@skku.edu; Tel: +82-31-299-4824; Fax: +82-31-290-7830.

GeunHyung Kim, Ph.D: Department of Bio-Mechatronic Engineering, College of Biotechnology and Bioengineering, Sungkyunkwan University, Suwon, South Korea. E-mail: gkimbme@skku.edu; Tel: +82-31-290-7828; Fax: +82-31-290-7830.

RSC Advances Accepted Manuscript

Abstract

Electrospun poly(ε-caprolactone) micro/nanofibers have been used widely for tissue regeneration. However, their low three-dimensional (3D) shape-ability, difficult macro-pore-structure controllability, and relatively low bioactivities have been major obstacles to their use as various tissue regenerative scaffolds. In this study, we present a new 3D fibrous scaffold in which the macrosized pore structure was manipulated using an electrohydrodynamic jet process supplemented with *in vitro* mineralization to obtain a hydroxyapatite (HA) layer in simulated body fluid (SBF). The fabricated scaffolds were a mesh-like structure (average diameter of fiber bundles: 342 ± 36 μm; average diameter of microfiber: 8.5 ± 1.2 μm) with high porosity (>91%), macro-pore size (368 ± 16 μm), and 100% interconnected pores. The HA particles on the surface of the scaffolds were well developed after a 7-day incubation in SBF, and the 3D fibrous scaffolds showed markedly higher and more homogenous HA deposition compared with that of control scaffolds fabricated with solid free-form fabrication, due to the larger surface area of fibrous bundles. The mineralized scaffolds were analyzed in terms of various physical and biological properties (water and protein absorption, mechanical properties, cell viability, DAPI/phalloidin staining, and osteogenic gene expression). Protein and water absorption of the fibrous scaffolds at 12 h were ~2.5-fold and ~2.3-fold greater than those of control scaffolds. Additionally, proliferation of viable cells (MC3T3-E1 pre-osteoblasts) on the 3D fibrous scaffold improved significantly compared to the control. The osteogenic gene expression (alkaline phosphatase activity and calcium mineralization) levels of the fibrous scaffolds were significantly enhanced compared with those of control scaffolds.

RSC Advances Accepted Manuscript

Introduction

Suitably designed biomedical scaffolds are necessary to successfully regenerate damaged tissues and organs. Consensus requirements for an ideal scaffold are: (1) favorable biocompatibility, (2) appropriate mechanical properties to withstand environmental stress and sustain neo-tissues, (3) well-balanced biodegradability with neo-tissues and mechanical sustainability, and (4) a highly porous structure to allow cell infiltration/migration and efficient transfer of nutrients and metabolic waste. Various types of scaffolds have been fabricated using solid-freeform fabrication to obtain layer-by-layered pore-structure, phase-separation, freeze-drying, self-assembly, and electrospinning to obtain micro/nanofibers and satisfy the fundamental requisites.[1-3] Of the biomaterials fabricated with these methods, micro/nanofibers are ideal because of their intrinsic structural similarity with the extracellular matrix (ECM), high porosity, and high surface area, which facilitate high cell attachment sites, rapid cell proliferation, and differentiation. Thus, electrospun micro/nanofibers have been used widely for regeneration of bone,[4] cartilage,[5] nerve,[6] skin,[7] and tendons.[8] However, although the micro/nanofibrous scaffolds provide advantages to seeded cells, the low controllability of pore structure (macro-pore size and porosity) and controllable three-dimensional (3D) shape-ability have limited their application. Generally, the macro-pore-size of scaffolds affects cell attachment/proliferation and differentiation. According to Murphy et al., a scaffold consisting of collagen/glycosaminoglycan with a small pore size exhibited an increased initial cell (MC3T3-E1) attachment rate, but a scaffold with a large pore size exhibited enhanced cell migration due to moderation of cell aggregation.[9] The resulting scaffolds had a pore size of 325 μm and showed high cellular activities including cell proliferation.[9] Therefore, appropriate means of generating a controllable macro-pore structure for scaffolds must be developed.

Various methods of fabricating 3D micro/nanofibrous scaffolds have been proposed. According to Lim et al.,[10] methods to fabricate 3D fibrous scaffolds are categorized into several types: salt or polymers (water soluble poly(ethylene oxide) and gelatin) leaching,[11, 12] wet-electrospinning using a bath collector containing ethanol,[13] electrospinning using ice crystals as a collector,[14] femtosecond laser ablation for structuring electrospun fiber mats,[15, 16] and a composite consisting of a mixture of nanofibers and microfibers.[17] In recent, 3D poly(ε-caprolactone) (PCL) nanofiber scaffold was

RSC Advances Accepted Manuscript

fabricated using noobing and weaving techniques and was composed of sheet-like multiaxial non-crimp fabrics.[18] In the scaffold, human adipose-derived stem cells were well controlled by topographic cues on the layer-by-layered nanofiber mats. Additionally, 3D zein and poly(ethylene glycol) electrospun fibrous structures with randomly oriented micro/nanofibers and large interconnected pore structure were obtained by decreasing the surface resistivity.[19]

However, the most methods of generating 3D micro/nanofibrous structures have been supplemental accumulation of electrospun fibrous mats, so that those cannot enable the controllable macro-pore structure of the stacked fibrous structures. [20]

In recent, we demonstrated a new technique using a combination of solid-freeform fabrication and a wet-electrohydrodynamic-jet process (EJP) to obtain a pore-controlled 3D PCL fibrous structure.[21] In this study, we mainly investigated the effect of various fabricating parameters (surface tension of target media, flow rate of feed, applied electric field, and weight fraction of solution) on process-ability in terms of generating a 3D macro-pore-controlled fibrous structure.

Here, we show the feasibility of the 3D fibrous scaffold for bone tissue regeneration using MC3T3-E1 pre-osteoblast cells. Although the 3D fibrous scaffolds provided a unique pore structure with highly macro-porous pores and 100% pore interconnectivity to enhance cellular activities, use of the fibrous PCL component only was insufficient to achieve the desired cellular responses. Thus, we treated the scaffold with two additional processes: (1) plasma treatment and (2) *in vitro* mineralization, as PCL is highly hydrophobic and lacks osteogenic properties. After the plasma treatment, the scaffolds showed enhanced hydrophilicity and were soaked in 1× simulated body fluid (SBF) for 7 days to facilitate development of a hydroxyapatite (HA) layer on the surface of the fibrous structure. HA is an essential inorganic material for bone tissue regeneration because of its outstanding ability to promote bone substitution and repair [22, 23]. The fabricated 3D PCL/HA fibrous scaffolds were analyzed in terms of surface morphology, surface chemical composition, water absorption, protein absorption, and mechanical stability. In addition, we characterized *in vitro* bioactivities, such as cell metabolic activity and osteogenic differentiation compared with a solid-free-form fabricated scaffold (control) treated with the same processes (plasma treatment and *in vitro* mineralization) with similar geometric

RSC Advances Accepted Manuscript

parameters (pore and strut size).

Experimental

Materials and fabrication of 3D scaffolds

PCL (density = 1.135 g cm^{-3}; M_w = 60 000; melting point = 60°C) was purchased from Sigma-Aldrich (St. Louis, MO, USA). A schematic of the fabrication process for the 3D electrospun fibrous scaffold (F-scaffold) is described in Fig. 1. We used a direct EJP in which ethanol solution was used as the target medium and the initial jet of electric-field-applied PCL solution was immersed directly in ethanol. The immersed single-jet solution was scattered into entangled microfibrous bundles in the ethanol.[21] The fibrous structures were lyophilized using a freeze dryer (SFDSM06; Samwon, Busan, South Korea) at –76°C for 1 day. The EJP was highly dependent on the surface tension of the target medium (ethanol), the PCL solution supply rate, and the weight fraction of the PCL solution. More details of the processing parameters were described in our previous study. [21]

We fixed the processing parameters at 10 wt% PCL solution, 1.9 kV/cm electric field, 0.2 ml/h PCL feed rate, 4-mm height of ethanol in the target bath, and 10 mm/s nozzle speed, which were controlled using a three-axis robot system (DTR3-2210-T-SG, DASA Robot, Seoul, South Korea). The 3D structure consisting of fibrous bundles was drawn using the robot system. The feeding rate of the PCL solution was controlled with a syringe pump (KDS 230; KD Scientific, Holliston, MA, USA). A power supply (SHV300RD-50K; Convertech, Seoul, South Korea) was used to provide the electric field.

PCL powder was inserted into a heating barrel (115°C) of the plotting system to fabricate control scaffolds (SFF-scaffold). The extruded microsized struts were pressed on the previously plotted struts, so the gap between the nozzle tip (diameter = 250 μm) and the previous layer was ~90% that of the extruded struts. The nozzle moving speed and pneumatic pressure were set to 7 mm s^{-1} and 675 ± 26 kPa, respectively.

Plasma treatment of the scaffolds

The dried fibrous scaffolds were treated with oxygen-plasma using low-frequency plasma (CUTE-

RSC Advances Accepted Manuscript

MP/R; Femto-Science, Inc., Seoul, Korea). A low frequency of 50 kHz, power of 40 W, and pressure of 5.3×10^{-1} Torr were used. The plasma chamber was cleaned by running a cycle with no sample for 30 min to remove any impurities. The fibrous structure was placed in the chamber and subjected to a plasma-exposure time of 30 min.

In vitro mineralization of the scaffolds in SBF

The plasma-treated PCL scaffolds were immersed in 1× SBF composed of NaCl (7.995 g), KCl (0.224 g), $CaCl_2 \cdot 2H_2O$ (0.368 g), $MgCl_2 \cdot 6H_2O$ (0.305 g), K_2HPO_4 (0.174 g), $NaHCO_3$ (0.349 g), and $Na_2SO_4 \cdot 10H_2O$ (0.161 g) in 1-L distilled water.[24] The pH of the solution was adjusted to 7.4 by adding Tris-HCl. The scaffolds were dipped in the SBF and incubated at 37°C for 7 days. The scaffolds were then washed with deionized water to remove adsorbed minerals, and lyophilized.

Characterization of the hybrid scaffolds

The surface morphology of the scaffolds was characterized by scanning electron microscopy (SEM) (SNE-3000M, SEC Inc., Seoul, South Korea) and an optical microscope (Model BX FM-32; Olympus, Tokyo, Japan) connected to a digital camera. Pore size was defined as the distance between the fibrous bundles and was measured on SEM images. Scaffold porosity was determined using the following equation: porosity (%) = $[(1 - W/V\rho)] \times 100$. In the equation, ρ is the density of the *in vitro* mineralized scaffold, which was calculated using the rule of mixture, and W and V mean the weight and volume of the scaffold, assuming a rectangular shape, respectively. The densities of PCL and HA were 1.145 g/cm^3 and 3.16 g cm^{-3}. [25]

Thermogravimetric analysis (TGA) was conducted under nitrogen using a TGA-2050 (TA-Instruments, New Castle, DE, USA). A typical sample mass of 10 mg was heated from 30 ^{o}C to 800 ^{o}C at a ramp rate of 20 ^{o}C min^{-1}.

The chemical bonding states and atomic concentrations in the scaffolds before and after plasma treatment were assessed by X-ray photoelectron spectroscopy (ESCA2000; VG Microtech, Uckfield, UK) using a hemispherical electrostatic energy analyzer and an Al K_α (1486.6 eV) X-ray source. The

RSC Advances Accepted Manuscript

base pressure in the sample chamber was controlled to 10^{-9} Torr. The measured spectra were displayed as plots of the number of electrons vs. the electron binding energy at a fixed, small energy interval. Peak area and peak height sensitivity factors were used for quantification. All surface compositions are expressed as atm%.

A Fourier-transform infrared (IR) spectrometer (model 6700; Nicolet, West Point, PA, USA) was used to assess the chemical components of the mineralized scaffold surface. IR spectra represent the mean of 30 scans at 600–4000 cm^{-1} at a resolution of 8 cm^{-1}.

To quantify the crystallite size of the *in vitro* mineralized HA on the scaffold surface, wide-angle X-ray diffraction (Siemens D 500 WAXD, Munich, Germany) with CuK_α radiation under beam conditions of 40 kV and 20 mA with collection of a spectrum at $2\theta = 5° – 40°$ and a step size of 0.1° was performed.

Water absorption was assayed by weighing the scaffolds before and after immersion in distilled water for 12 h. Water absorption (%) was calculated using the equation, $(W_f - W_o)/W_o \times 100$, where W_f is the weight of scaffolds after 12 h, and W_o is the initial weight.

Five samples of each scaffold were cut into small strips for assessment of their mechanical properties. A tensile and compression test was carried out using a universal tensile machine (Top-tech 2000; Chemilab, Seoul, South Korea). The stress–strain curves for the scaffolds were recorded at a stretching and compression speed of 0.5 mm s^{-1}. All values are means ± standard deviation (SD) (n = 5).

Protein absorption was measured using the bicinchoninic acid (BCA) protein assay (Pierce Kit; Thermo Scientific, Waltham, MA, USA). Scaffolds (10×10 mm^2) were placed in 24-well plates containing α-minimum essential medium (α-MEM) and 10% fetal bovine serum (FBS) (Gemini Bio-Products, Calabasas, CA, USA) and incubated at 37°C for 1, 6, and 12 h. Samples were washed with PBS and lysed with 0.1% Triton X-100. An aliquot of the lysate (25 μL) was added to 200 μL of BCA working reagent, and the mixture was incubated for 30 min at 37°C. Absorbance at 562 nm was determined using a plate reader. Samples incubated in serum-free medium were used as blanks. Protein adsorption values are presented as means ± SD ($n = 5$).

RSC Advances Accepted Manuscript

In vitro cell culture

The scaffolds measuring 5 × 5 mm^2 were prepared and sterilized using 70% ethanol for 1 h with a 2-h ultraviolet light application prior to overnight incubation in culture medium. Mouse pre-osteoblast cells (MC3T3-E1; ATCC, Manassas, VA, USA) were cultured in the scaffolds and maintained in α-MEM (Life Sciences, Carlsbad, CA, USA) containing 10% FBS and 1% antibiotic-antimycotic (Cellgro, Herndon, VA, USA). The cells were seeded onto the scaffolds at a density of 1×10^5 per specimen and incubated under an atmosphere of 5% CO_2 at 37℃, with medium exchange every second day.

Proliferation of viable cells was determined by the MTT assay (Cell Proliferation Kit I; Boehringer Mannheim, Mannheim, Germany). This assay is based on cleavage by mitochondrial dehydrogenases in viable cells of the yellow tetrazolium salt, MTT, to produce purple formazan crystals. Cells on the surface were incubated with 0.5 mg/mL MTT for 4 h at 37℃. Absorbance at 570 nm (λ_{570}) was measured using a microplate reader (EL800; BioTek Instruments, Winooski, VT, USA). Five samples were tested per incubation period, and each test was performed in triplicate.

After incubation for 7 and 14 days, the scaffolds were subjected to staining with DAPI and phalloidin to visualize nuclei and the actin cytoskeleton. The number of cells per mm^2 and area fraction (%) of actin identified by DAPI and phalloidin staining, respectively, were measured on surface fluorescence images of the composite scaffolds using the ImageJ software.

Alkaline phosphatase (ALP) activity and Alizarin Red-S staining

ALP activity was assayed by measuring the release of *p*-nitrophenol from *p*-nitrophenyl phosphate (*p*-NPP). Scaffolds seeded with MC3T3-E1 cells were rinsed gently with PBS and incubated in Tris buffer (10 mM, pH 7.5) containing 0.1% Triton X-100 for 10 min. Aliquots of the lysate (100 μL) were added to 96-well tissue culture plates containing 100 μL of *p*-NPP solution, prepared using an ALP kit (procedure no. ALP-10; Sigma-Aldrich). In the presence of ALP, *p*-NPP is transformed to *p*-nitrophenol and inorganic phosphate. ALP activity was determined by measuring absorbance at 405

RSC Advances Accepted Manuscript

nm (λ_{405}) using a microplate reader (Spectra III; SLT-Lab Instruments, Salzburg, Austria).

Calcium mineralization of the samples was determined by Alizarin Red-S staining of MC3T3-E1 cells in 24-well plates. The cells were cultured in α-MEM containing 50 μg mL^{-1} vitamin C and 10 mM β-glycerophosphate. The cells were then washed three times in PBS, fixed in 70% (v/v) cold ethanol (4°C) for 1 h, and air dried. The ethanol-fixed specimens were stained with 40 mM Alizarin Red-S (pH 4.2) for 1 h and washed three times with purified water. The samples were then destained with 10% cetylpyridium chloride in 10 mM sodium phosphate buffer (pH 7.0) for 15 min. An optical microscope was used to observe the staining.

Total protein content

Total protein content was measured by the BCA protein assay (Pierce kit; Thermo Scientific). Scaffolds were washed with PBS and lysed with 1 mL of Triton X-100 (0.1%). An aliquot of the lysate (25 μL) was added to 200 μL of BCA working reagent, and the mixture was incubated for 30 min at 37℃. Protein concentration was determined from the absorbance at 562 nm (λ_{562}) measured using an enzyme-linked immunosorbent assay reader and converted to the total protein concentration using a standard curve.

Statistical analyses

All data are presented as means ± SDs. Statistical analyses were performed using the SPSS software ver. 20.0 (SPSS, Inc., Chicago, Il, USA). Statistical analyses consisted of single-factor analyses of variance. A $p < 0.05$ was considered to indicate significance.

Results and discussion

Scaffold fabrication and characterization

Biomedical scaffolds should comprise well-connected pores of an appropriate size because pore connectivity affects the rate of bone deposition and cell infiltration.[26] The appropriate pore size for

RSC Advances Accepted Manuscript

hard tissue regeneration is > 300 μm.[27, 28] Based on these studies, we fabricated multi-layered scaffolds with pore sizes of 400–500 μm and a cross-hatched structure to the thickest direction to achieve high cellular activities.[28] The fabricated 3D fibrous scaffolds (F-scaffold), which consisted of microfibers 8.1 ± 1.7 μm in diameter and a control scaffold having a similar pore structure, which was fabricated using the melt-plotting method, are shown in Fig. 2(a, b).

The fabricated PCL fibrous scaffolds were treated with oxygen plasma to modify the surface chemical components, resulting in a hydrophilic scaffold. This can lead to efficient HA development on the scaffold surface due to the easy wettability of the scaffolds in the SBF solution. The chemical composition and relative areas corresponding to the various chemical bonds before and after plasma treatment of the F scaffold are shown in Table 1. The surface chemical composition before treatment was 26.3% oxygen and 73.7% carbon, compared to 38.8% oxygen and 61.2% carbon after plasma exposure. Therefore, the increase in the surface oxygen content after plasma treatment likely enhanced the surface hydrophilicity of the fibrous scaffolds.

Various bioceramics (HA, calcium phosphate, and bioglass) have been investigated, and can facilitate rapid osteogenesis because of their similar chemical composition to the mineral components of bone. In particular, HA has been used widely in bone cement for craniofacial defect repairs[29] and as a coating agent for femoral constituents during hip replacement.[30]

The plasma-treated fibrous structures were submerged in SBF for 7 days to allow HA attachment. The 7 day soaking time was fixed because the longer immersion time can cause to block the pores of the scaffold. Martuinez et al. observed changes in the formation of HA as the treatment time increased. After 1.5h of soaking in SBF, formation of spherical particles with diameters less than 1 μm was observed on the surface layer. However, a more complete coating was observed after 6 h of treatment. After 24 h of treatment in SBF, spherical particles with diameters exceeding 1 μm was observed. The spheres exceeded the diameter of 3 μm after 3 days soaking, but the situation previously described remained unchanged after 7 days of treatment although there was a more compact formation and larger particles were observed.[31] As shown in SEM images, HA particles developed on the surface of both scaffolds after *in vitro* mineralization [Fig. 2(c, d)]. Interestingly, the HA was sporadically

RSC Advances Accepted Manuscript

developed on the SFF-scaffold surface (control), while it covered the F-scaffold surface in a more homogeneous manner. The porosity values of the mineralized SFF- and F-scaffolds were 56% and 91%, respectively.

Fig. 3(a,b) shows the TGA graphs obtained from the thermograms of the F-scaffold and SFF-scaffold, respectively, before and after immersion in the SBF solution. The TGA graphs demonstrated that the pure PCL before the treatment in SBF decomposed in a single step, while the scaffolds after immersion in SBF showed 2-step degradation profile due to the developed HA component. The TGA data specified that the temperature of the degradation started at 350 ^{o}C due to the PCL component, and the remnant amount for the F-scaffold and SFF-scaffold at 700 ^{o}C was about 37.3% and 2.2%, respectively. From the result, we can estimate that the F-scaffold can provide much effective development of HA compared to the control (SFF-scaffold).

IR and X-ray diffraction (XRD) were performed to determine qualitatively the HA composition. The IR spectra of the scaffolds before and after immersion in SBF are shown in Fig. 4(a, b). The absorption band at 1732 cm^{-1} was contributed by the carboxyl group of PCL. The presence of HA ($Ca_{10}(PO_4)_6(OH)_2$) was indicated by absorption peaks due to vibrational modes of the phosphate and hydroxyl groups. Asymmetric stretching vibration of the phosphate group (PO_4^{-3}) is indicated by a strong band at 1000–1150 cm^{-1}.[32] Crystalline HA produced two characteristic OH bands near 3337 and 630 cm^{-1}; the OH stretching vibration is unique to crystalline HA.[32] Comparing the spectra before and after surface mineralization, the peak at 1032 cm^{-1} was due to PO_4^{-3} vibrations, and the broad band at 3100–3600 cm^{-1} was due to the OH groups of the HA particles and absorbed water. [33]

The XRD results for the F- and SFF-scaffolds are shown in Fig. 4(c, d). According to Jayakumar *et al*.,[24] the diffraction peaks (2θ = 31.8° and 40.8°) were due to the (211) and (310) plane of HA, and the intensity of the (211) plane in the F-scaffold was higher than that in the SFF-scaffold, indicating effective HA crystallization. The mean crystallite size of the HA on the F- and SFF-scaffolds was determined by measuring the full-width at half-maximum (FWHM) at plane (211). Size was calculated using the Scherer equation,[34] $0.89\lambda/(\beta \cos\theta)$, where λ, β, and θ are the wavelength (0.154 nm) of Cu K_{α}, the FWHM of the plane (211), and the diffraction angle of the plane (211),

RSC Advances Accepted Manuscript

50respectively. The crystallite size (0.49 nm) of the plane (211) of the F-scaffold was significantly larger than that (0.30 nm) of the SFF-scaffold, indicating that the crystallite size of the plane on the surface of the F-scaffold developed more efficiently in the SBF solution due to the enlarged surface area of the micro-fibrous bundles.

Mechanical properties

The mechanical properties of scaffolds are an important design parameter because implanted scaffolds must endure the external mechanical stresses due to various environmental conditions in the implanted area. The mechanical properties of scaffolds influence the morphology and bioactivities of the cultured cells. [35, 36]

The F- and SFF-scaffolds were cut and stretched using a tensile tester at a speed of 0.5 mm s^{-1} and compressed with a speed of 0.5 mm s^{-1} in a dry state to evaluate their mechanical properties before and after *in vitro* mineralization. Figure 5 (a, b) shows the tensile and compression strength results before and after mineralization of the F- and SFF-scaffolds. The F-scaffold showed a tensile (compression) modulus of 0.1 ± 0.03 MPa (0.3 ± 0.1 kPa) before and 0.25 ± 0.03 MPa (2.4 ± 0.6 kPa MPa) after, and maximum tensile stress of 0.03 ± 0.004 MPa before and 0.06 ± 0.002 MPa after mineralization. The tensile (compression) modulus for the SFF-scaffold before was 18.03 ± 1.4 MPa (5.6 ± 0.3 MPa MPa) and that after was 18.4 ± 0.6 MPa (5.9 ± 1.5 MPa); the maximum tensile stress was 2.95 ± 0.26 MPa before and 3.34 ± 0.08 MPa after mineralization. Peter Zioupos et al. measured the modulus of trabecular bone, and the result indicated that the modulus was 0.76 ± 0.39 GPa.[37] As shown in the result, the mechanical properties of the both scaffolds were still poor compared to real cortical and trabecular bone. In addition, the F-scaffold has significantly low mechanical properties compared to SFF scaffold due to the high porosity. In general, the modulus is significantly correlated with the material's porosity, and the correlation for the modulus and porosity has been expressed as an equation, $E(\phi) = E_o (1 - \phi^{2/3})$.[38] In this equation, E_o is the modulus of a material without any pores and ϕ is the porosity, and the pores can be assumed to be cubic shape. In addition, the modulus and maximum tensile stress of the F-scaffold were meaningfully enhanced after *in vitro* mineralization (*p*

RSC Advances Accepted Manuscript

< 0.05). J. Xie et al. demonstrated that HA coatings evidently improved the mechanical properties of PCL scaffolds.[39] An improved modulus of F-scaffold is typical for a composite system because the large amount of HA particles reinforces the fibrous structure, while for the SFF-scaffold the effect of the HA particles on the mechanical properties was negligible due to the significantly low amount of HA particles.

The relation between the modulus of PCL and HA can be analyzed using the following simple rule of mixture, $E = E_p\beta_p + E_H\beta_H$. In this equation, E_p and E_H are the moduli of pure PCL and HA, respectively, and β_p and β_H are the volume fractions of the PCL and the HA, respectively. Similar results were reported by Lie et al. [40] In their study, the modulus was improved substantially by increasing the immersion times of electrospun poly(lactic-co-glycolic acid) nanofibers in the SBF solution.

Water and protein absorption

Water absorption is an important factor for scaffolds as it represents the absorption ability of the biological solution and transfer of nutrients and metabolic waste within the biomaterials, resulting in enhanced cellular activities, such as proliferation and metabolic activity.[41]

Figure 6(a) shows water absorption on the F- and SFF-scaffolds prior to HA mineralization (i.e. only after plasma treatment). The water absorption on the F-scaffold was greater than SFF-scaffold due to the fibrous bundles. Figure 6(b) shows the water absorption abilities of the mineralized SFF and F-scaffolds. The F-scaffold showed greater water absorption ability compared to the SFF-scaffold due to the well-developed and homogeneously distributed HA particles in the F-scaffold.

The protein absorption ability of biomedical scaffolds can impact cell attachment and proliferation due to the absorption cell-binding proteins (fibrinogen, fibronectin, and vitronectin).[42] According to several reports,[43, 44] absorption of proteins is related to surface topography, chemical composition, and hydrophobicity.

Figure 6(c and d) displays the protein absorption of F-scaffold and SFF-scaffold before and after *in vitro* mineralization, respectively. As shown in the result, the ability of protein absorption for the

RSC Advances Accepted Manuscript

mineralized scaffolds was significantly improved compared with that of the scaffolds before the mineralization. This phenomenon was because of the HA component in the scaffold. [45]

Protein absorption (μg/mm^3) to the mineralized F- and SFF-scaffolds was measured at 1, 6, and 12 h (Fig. 6(d)). Protein absorption by the F-scaffold at 6 and 12 h was significantly greater than that of the SFF-scaffold ($p < 0.05$). This was likely due to the fibrous structure of the F-scaffold, which provided a significantly greater surface area compared to the micro-strut based (SFF) scaffold. Therefore, we speculate that the F-scaffold exhibited higher initial cell attachment and proliferation than the SFF-scaffold.

In vitro *cellular activities*

Proliferation of pre-osteoblasts on the three scaffolds (F- and SFF-scaffolds, which were mineralized *in vitro* for 7 days, and another F-scaffold before the mineralization) was characterized by MTT assay. The numbers of cells on the mineralized F-scaffold (M-F-scaffold) at 1, 3, and 7 days were significantly higher than those on the non-mineralized F-scaffold (NM-F-scaffold) and mineralized SFF-scaffold (M-SFF-scaffold) ($p < 0.05$; Fig. 7(a)). Additionally, the proliferation rate can be higher on the M-F-scaffold than on the NM-F-scaffold and M-SFF-scaffold, for two important reasons. First, the greater surface area and porosity of the M-F-scaffold, which provided larger cell-attachment sites compared to the M-SFF-scaffold; second, the homogeneously mineralized HA particles from which calcium and phosphorous ions are released during the incubation. According to Chen et al., calcium and phosphorus ions stimulate the proliferation and differentiation of osteoblast-like-cells (MG63).[46, 47]

Immunofluorescence and SEM

Immunofluorescence images M-F- and M-SFF-scaffolds on days 7 and 14 of cell culture are shown in Fig. 7 (b, c). Blue and red represent nuclei and F-actin, respectively. F-actin was spread evenly across the surface of the microsized struts of the M-SFF scaffold, similar behavior on a flat surface. However, the cells on the M-SFF-scaffold were not distributed homogeneously across the entire scaffold (please see the image describing 1st and 2nd layers of the Fig. 7(b)). In contrast, the F-actin on the M-F-

RSC Advances Accepted Manuscript

scaffold was thin and stretched aligned to the fibrous structure, and was distributed homogeneously across the entire scaffold. This phenomenon was more evident after 14 days of cell culture. At 14 days, nuclei and F-actin were distributed more widely on the M-F-scaffolds compared to the M-SFF-scaffolds. Figure 7(d, e) shows the number of nuclei per mm^2 and the area of F-actin, respectively, on the two scaffolds. Cell proliferation and cytoskeletal activity on the M-F-scaffold were significantly greater than those on the M-SFF-scaffold. The numbers of cells on the first and second layer struts in the thickness direction of the scaffolds was compared using immunofluorescence imaging, as shown in Fig. 7(b, c). As shown in Fig. 7(f), more homogeneous cell distribution between 1^{st} layer and 2^{nd} layer was observed on the M-F-scaffold on days 7 and 14 compared to the M-SFF-scaffold.

Based on these results, we conclude that the M-F-scaffold facilitates greater cell attachment and proliferation than the M-SFF-scaffold. This was due to the fibrous topological surface and well developed HA layer of the M-F-scaffold, which may function as cues for cell activation.

ECM mineralization on the scaffolds was quantified. SEM images of the M-F- and M-SFF-scaffolds after 7 and 14 days of culture are shown in Fig. 8(a, b). The M-F-scaffold exhibited greater cell density and a considerably denser matrix at 7 days compared to the M-SFF-scaffold. Additionally, cells in the M-F-scaffold were more packed within the well-developed mineralized matrix and showed extended lamellipodia at 14 days; in contrast cells in the M-SFF-scaffolds had not proliferated fully and the matrix had not developed sufficiently. This was due to the synergistic effect of surface topography, which can markedly affect cell behavior,[48] the fibrous structure, and the bioactivity of the more well developed HA on the M-F-scaffolds.

ALP activity and calcium mineralization

ALP activity is used widely as a marker of early osteoblastic differentiation. Thus, we measured ALP activity in MC3T3-E1 cells on both scaffold types to assess the influence of the fibrous structure and *in vitro* mineralization on early stage differentiation of cultured cells. ALP activity was normalized to the total protein content (Table 2). Relative ALP activity of MC3T3-E1 cells on the scaffolds for 7 and 14 days is shown in Fig. 9(a). The ALP activity of cells on the M-F-scaffold was significantly higher ($p < 0.05$) on both days than those of cells on the NM-F-scaffold and the M-SFF-scaffold.

RSC Advances Accepted Manuscript

An Alizarin Red-S assay was conducted on days 7 and 14 to evaluate calcium mineralization of the matrix. To remove the effect of *in vitro* mineralized component (HA) in the M-SFF and M-F-scaffolds on the Alizarin Red-S assay, a control experiment for the mineralized scaffolds, which were incubated in the medium for 7 and 14 days without cells under the same cell-culturing process, was conducted. The measured OD value of the M-SFF and M-F-scaffolds incubated without cells was deducted from the OD values of the scaffolds, which were cultured with the cells. Figure 9(b) shows that calcium mineralization was considerably higher on the M-F-scaffolds ($p < 0.05$) than on the NM-F-scaffold and M-SFF-scaffolds. Alizarin Red-S–stained micrographs are shown in Fig. 9(c, d). Staining intensity on both scaffold types increased with increasing culture time from 7 to 14 days. Dense red spots were distributed sporadically in the M-SFF-scaffolds, but were distributed more homogeneously on the M-F-scaffolds, the pores of which were filled evenly with cells/ECM. This resulted in greater mineralized matrix deposition of M-F-scaffold. Therefore, the M-F-scaffold exhibited enhanced cell proliferation and differentiation compared to the NM-F-scaffold and the M-SFF-scaffold.

Conclusion

A 3D fibrous PCL scaffold consisting of multi-layered microfiber bundles was fabricated using an EJP. HA particles developed on the surface of the 3D fibrous scaffolds after immersion in SBF for 7 days. The new fibrous PCL/HA scaffolds were characterized with regard to various physical and biological properties. Protein and water absorption was enhanced significantly due to the enlarged surface area and greater number of HA particles on the F-scaffolds. Cell proliferation, ALP activity, and calcium mineralization levels on the fibrous scaffolds were enhanced significantly compared to those of the control scaffold. These results suggest that the mineralized 3D fibrous scaffolds can be used for tissue regeneration.

Acknowledgements

This research was financially supported by the National Research Foundation of Korea grant funded by the Ministry of Education, Science, and Technology (MEST) (Grant No. NRF-

RSC Advances Accepted Manuscript

2012R1A2A2A01017435) and also was partially supported by a grant of the Korean Health Technology R&D Project, Ministry of Health & Welfare, Republic of Korea (Grant no. A120942).

RSC Advances Accepted Manuscript

Reference

1. T. Lu, Y. Li and T. Chen, *International journal of nanomedicine*, 2013, 8, 337-350.

2. Y. Kim and G. Kim, *J Mater Chem B*, 2013, 1, 3185-3194.

3. M. Cicuendez, M. Malmsten, J. C. Doadrio, M. T. Portoles, I. Izquierdo-Barba and M. Vallet-Regi, *J Mater Chem B*, 2014, 2, 49-58.

4. H. Yoshimoto, Y. M. Shin, H. Terai and J. P. Vacanti, *Biomaterials*, 2003, 24, 2077-2082.

5. A. Thorvaldsson, H. Stenhamre, P. Gatenholm and P. Walkenstrom, *Biomacromolecules*, 2008, 9, 1044-1049.

6. L. Ghasemi-Mobarakeh, M. P. Prabhakaran, M. Morshed, M. H. Nasr-Esfahani and S. Ramakrishna, *Biomaterials*, 2008, 29, 4532-4539.

7. Q. L. Zhao, S. W. Wang, Y. Y. Xie, W. F. Zheng, Z. Wang, L. Xiao, W. Zhang and X. Y. Jiang, *Adv Healthc Mater*, 2012, 1, 560-566.

8. M. R. Ladd, S. J. Lee, J. D. Stitzel, A. Atala and J. J. Yoo, *Biomaterials*, 2011, 32, 1549-1559.

9. C. M. Murphy, M. G. Haugh and F. J. O'Brien, *Biomaterials*, 2010, 31, 461-466.

10. S. Zhong, Y. Zhang and C. T. Lim, *Tissue engineering. Part B, Reviews*, 2012, 18, 77-87.

11. A. G. Mikos, A. J. Thorsen, L. A. Czerwonka, Y. Bao, R. Langer, D. N. Winslow and J. P. Vacanti, *Polymer*, 1994, 35, 1068-1077.

12. B. M. Whited, J. R. Whitney, M. C. Hofmann, Y. Xu and M. N. Rylander, *Biomaterials*, 2011, 32, 2294-2304.

13. Y. Yokoyama, S. Hattori, C. Yoshikawa, Y. Yasuda, H. Koyama, T. Takato and H. Kobayashi, *Mater Lett*, 2009, 63, 754-756.

14. M. Simonet, O. D. Schneider, P. Neuenschwander and W. J. Stark, *Polym Eng Sci*, 2007, 47, 2020-2026.

15. H. W. Choi, J. K. Johnson, J. Nam, D. F. Farson and J. Lannutti, *J Laser Appl*, 2007, 19, 225-231.

16. M. S. Kim, J. Son, H. Lee, H. Hwang, C. H. Choi and G. Kim, *Curr Appl Phys*, 2014, 14, 1-7.

RSC Advances Accepted Manuscript

17. Q. P. Pham, U. Sharma and A. G. Mikos, *Biomacromolecules*, 2006, 7, 2796-2805.

18. J. W. Xie, B. Ma and P. L. Michael, *Adv Healthc Mater*, 2012, 1, 674-678.

19. S. B. Cai, H. L. Xu, Q. R. Jiang and Y. Q. Yang, *Langmuir : the ACS journal of surfaces and colloids*, 2013, 29, 2311-2318.

20. W. J. Lu, J. S. Sun and X. Y. Jiang, *J Mater Chem B*, 2014, 2, 2369-2380.

21. M. S. Kim and G. Kim, *Langmuir : the ACS journal of surfaces and colloids*, 2014, 30, 8551-8557.

22. H. Yoshikawa, N. Tamai, T. Murase and A. Myoui, *J R Soc Interface*, 2009, 6, S341-S348.

23. M. P. Prabhakaran, J. Venugopal and S. Ramakrishna, *Acta biomaterialia*, 2009, 5, 2884-2893.

24. S. Srinivasan, R. Jayasree, K. P. Chennazhi, S. V. Nair and R. Jayakumar, *Carbohydrate polymers*, 2012, 87, 274-283.

25. M. Wang, R. Joseph and W. Bonfield, *Biomaterials*, 1998, 19, 2357-2366.

26. K. A. Hing, S. M. Best, K. E. Tanner, W. Bonfield and P. A. Revell, *Journal of Biomedical Materials Research Part A*, 2004, 68A, 187-200.

27. C. M. Murphy, M. G. Haugh and F. J. O'Brien, *Biomaterials*, 2010, 31, 461-466.

28. M. Yeo, C. G. Simon and G. Kim, *J Mater Chem*, 2012, 22, 21636-21646.

29. F. D. Burstein, S. R. Cohen, R. Hudgins, W. Boydston and C. Simms, *Plast Reconstr Surg*, 1999, 104, 1270-1275.

30. C. J. Oosterbos, A. I. Rahmy, A. J. Tonino and W. Witpeerd, *Acta orthopaedica Scandinavica*, 2004, 75, 127-133.

31. A. Martinez, I. Izquierdo-Barba and M. Vallet-Regi, *Chem Mater*, 2000, 12, 3080-3088.

32. A. Stoch, W. Jastrzebski, A. Brożek, B. Trybalska, M. Cichocińska and E. Szarawara, *Journal of molecular structure*, 1999, 511, 287-294.

33. S. Z. Fu, L. L. Yang, J. Fan, Q. L. Wen, S. Lin, B. Q. Wang, L. L. Chen, X. H. Meng, Y. Chen and J. B. Wu, *Colloid Surface B*, 2013, 107, 167-173.

34. L. V. Azároff, *Elements of X-ray crystallography*, McGraw-Hill, New York,, 1968.

RSC Advances Accepted Manuscript

35. D. E. Discher, P. Janmey and Y. L. Wang, *Science*, 2005, 310, 1139-1143.

36. M. E. Gomes, J. S. Godinho, D. Tchalamov, A. M. Cunha and R. L. Reis, *M at Sci Eng C-Bio S*, 2002, 20, 19-26.

37. S. D. Ryan and J. L. Williams, *Journal of biomechanics*, 1989, 22, 351-355.

38. O. Ishai and L. Cohen, *International Journal of Mechanical Sciences*, 1967, 9, 539-546.

39. J. W. Xie, S. P. Zhong, B. Ma, F. D. Shuler and C. T. Lim, *Acta Biomater*, 2013, 9, 5698-5707.

40. W. Y. Liu, Y. C. Yeh, J. Lipner, J. W. Xie, H. W. Sung, S. Thomopoulos an d Y. N. Xia, *Langmuir : the ACS journal of surfaces and colloids*, 2011, 27, 9088-9093.

41. S. J. Hollister, *Nat Mater*, 2005, 4, 518-524.

42. J. M. Goddard and J. H. Hotchkiss, *Progress in Polymer Science*, 2007, 32, 6 98-725.

43. L. C. Xu and C. A. Siedlecki, *Biomaterials*, 2007, 28, 3273-3283.

44. Y. Tamada and Y. Ikada, *Journal of colloid and interface science*, 1993, 155, 334-339.

45. J. Huang, Y. W. Lin, X. W. Fu, S. M. Best, R. A. Brooks, N. Rushton and W. Bonfield, *Journal of Materials Science: Materials in Medicine*, 2007, 18, 2 151-2157.

46. Q. Chen, A. Efthymiou, V. Salih and A. Boccaccini, *Journal of biomedical ma terials research Part A*, 2008, 84, 1049-1060.

47. S. Fu, L. Yang, J. Fan, Q. Wen, S. Lin, B. Wang, L. Chen, X. Meng, Y. Ch en and J. Wu, *Colloids and surfaces. B, Biointerfaces*, 2013, 107, 167-173.

48. H. Jeon, C. G. Simon, Jr. and G. Kim, *Journal of biomedical materials resear ch. Part B, Applied biomaterials*, 2014, DOI: 10.1002/jbm.b.33158.

RSC Advances Accepted Manuscript

Tables

Table 1. XPS data before and after the plasma-treatment for the 3D fibrous scaffolds.

	Chemical composition (%)		Relative area corresponding to different chemical bonds (%)				
			Carbon			Oxygen	
Plasma-treatment	Carbon	Oxygen	C-H	C=O	-C-O-O	-OH	-COOH
Before	73.679	26.321	51.459	12.935	9.285	17.36	8.961
After	61.237	38.763	35.641	14.417	11.179	33.27	5.493

Table 2. Total protein contents of the samples.

Total protein content [mg]		
Samples	SFF-scaffold	F-scaffold
7 days	47.41± 6.7	63.09±6.34
14 days	101.0±16.65	125.52±37.32

RSC Advances Accepted Manuscript

Figures

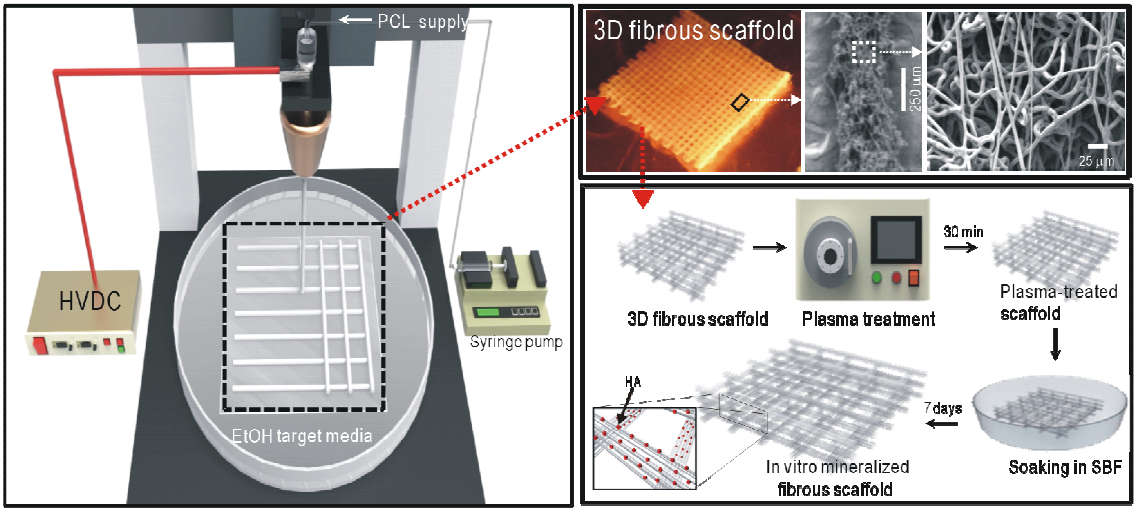

Figure 1. Schematic of generation of the three-dimensional (3D) fibrous scaffold, which was treated with plasma and mineralized in 1 × simulated body fluid (SBF).

RSC Advances Accepted Manuscript

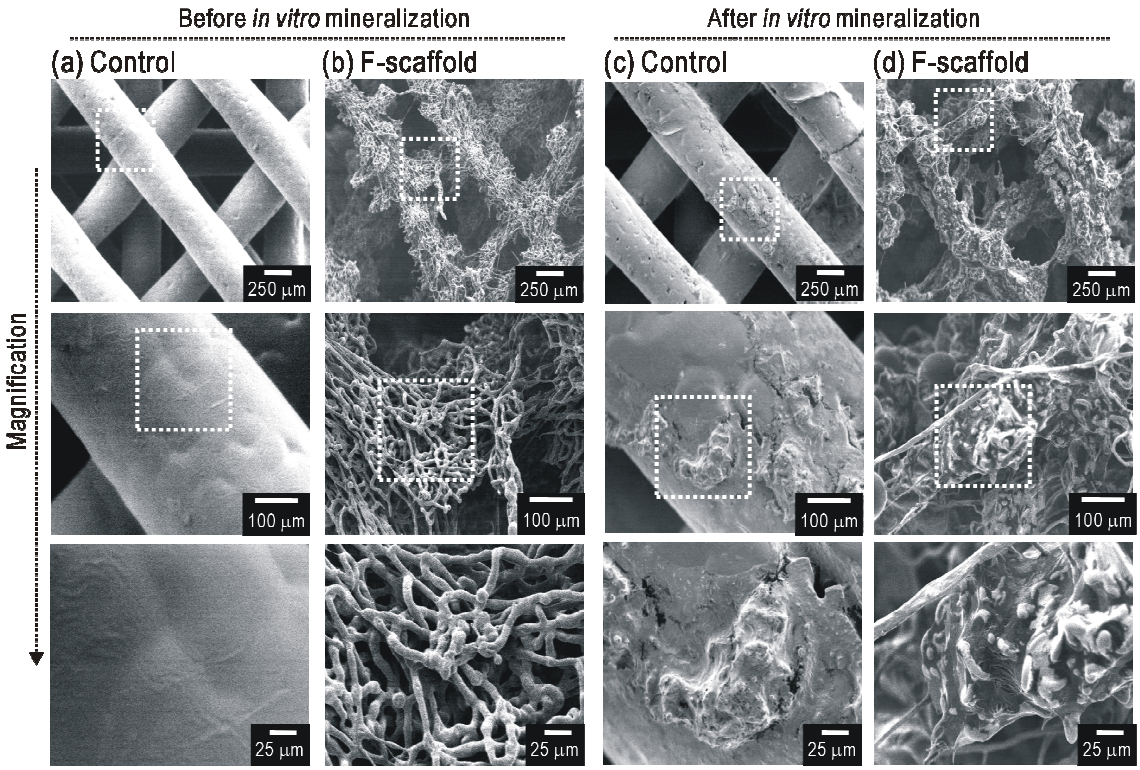

Figure 2. Scanning electron micrographs before and after *in vitro* mineralization of the (a, c) control scaffold (SFF-scaffold), and (b, d) fibrous scaffold (F-scaffold).

RSC Advances Accepted Manuscript

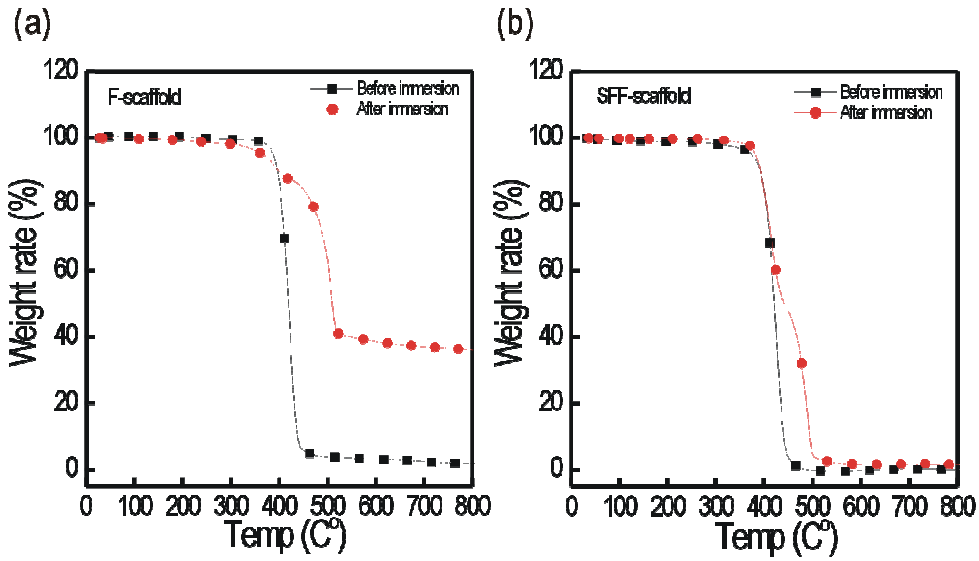

Figure 3. Thermogravimetric analysis of (a) F-scaffold and (b) SFF-scaffold before and after *in vitro* mineralization.

RSC Advances Accepted Manuscript

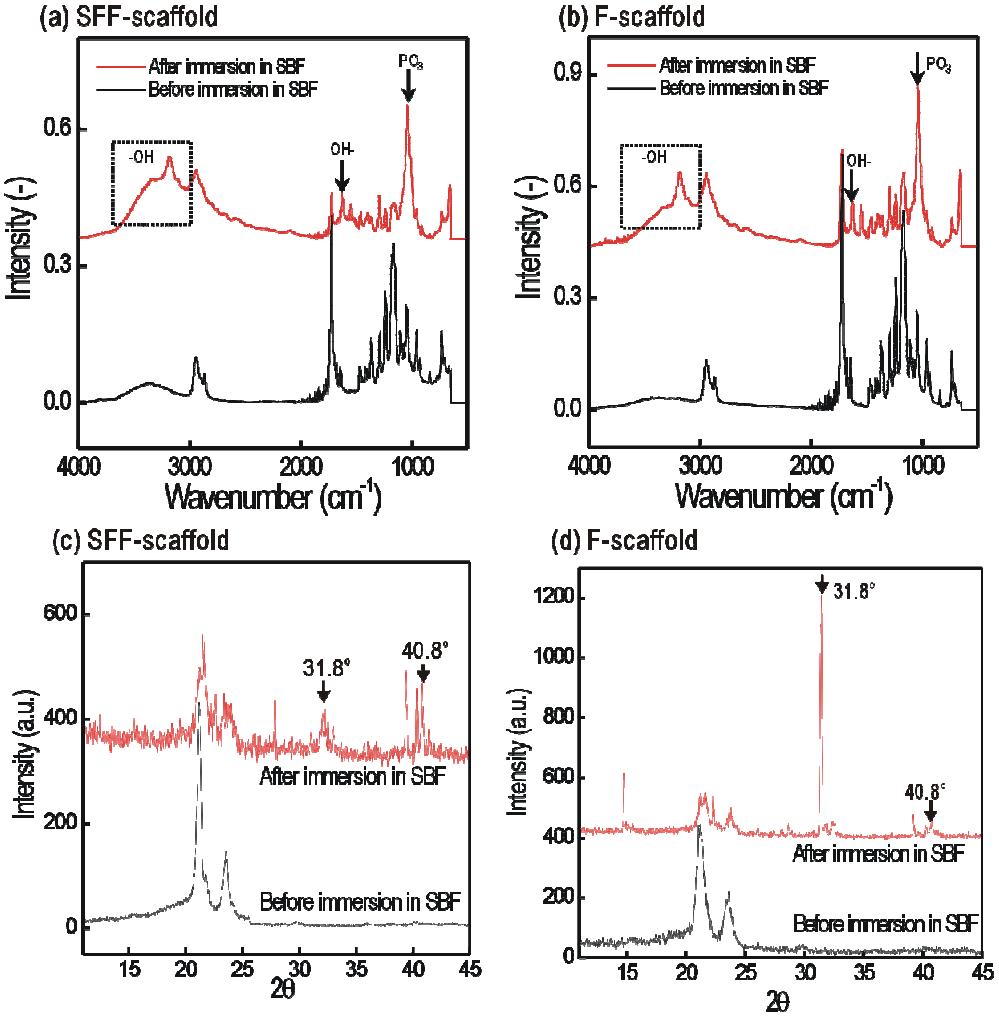

Figure 4. Fourier transform infrared spectra before and after *in vitro* mineralization of the (a) SFF scaffold and (b) F-scaffold. Mineralization was achieved by incubation for 7 days. X-ray diffraction patterns of the (c) SFF and (d) F-scaffolds before and after mineralization.

RSC Advances Accepted Manuscript

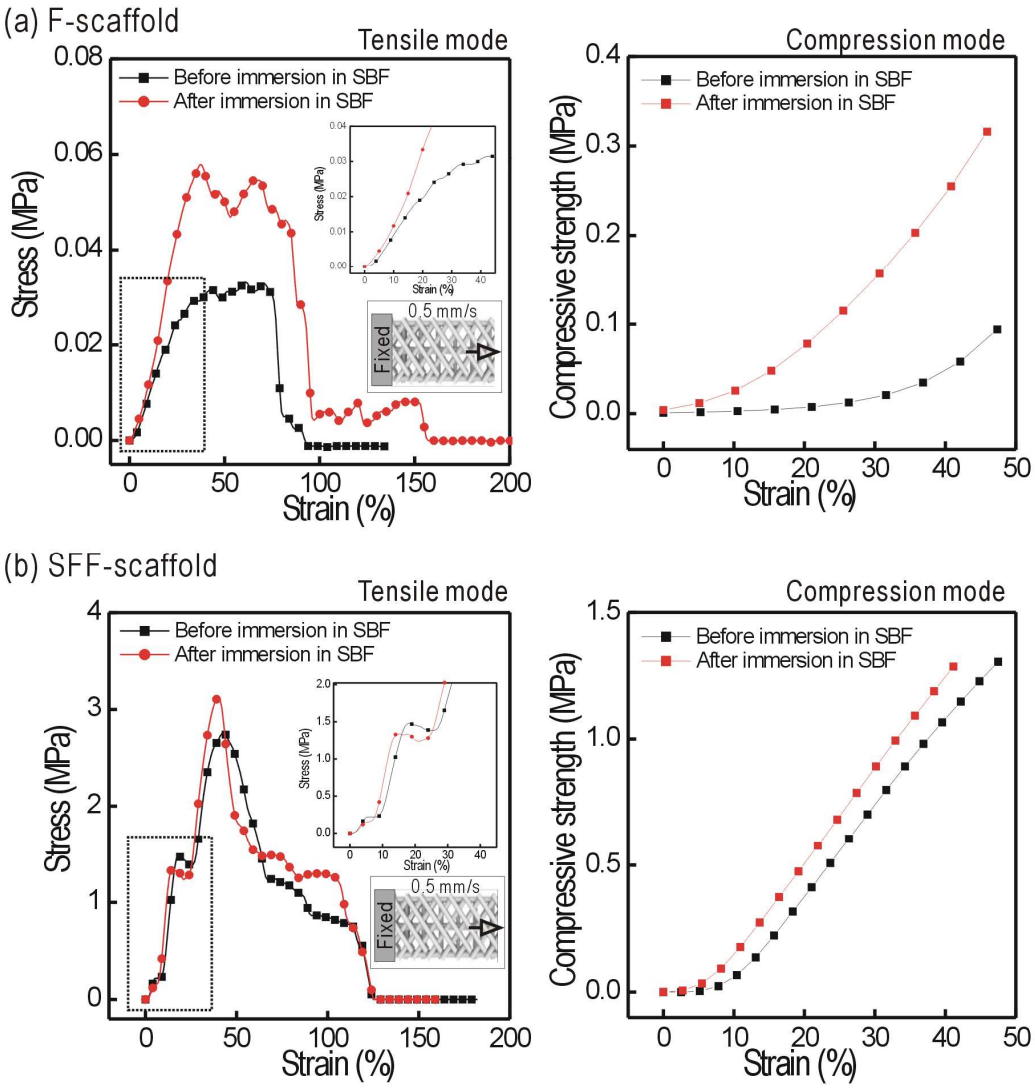

Figure 5. Stress–strain curves generated using tensile (stretching rate of 0.5 mm s^{-1}) and compression mode (compression rate of 0.5 mm s^{-1}) and for the (a) F-scaffold and (b) SFF-scaffold before and after *in vitro* mineralization.

RSC Advances Accepted Manuscript

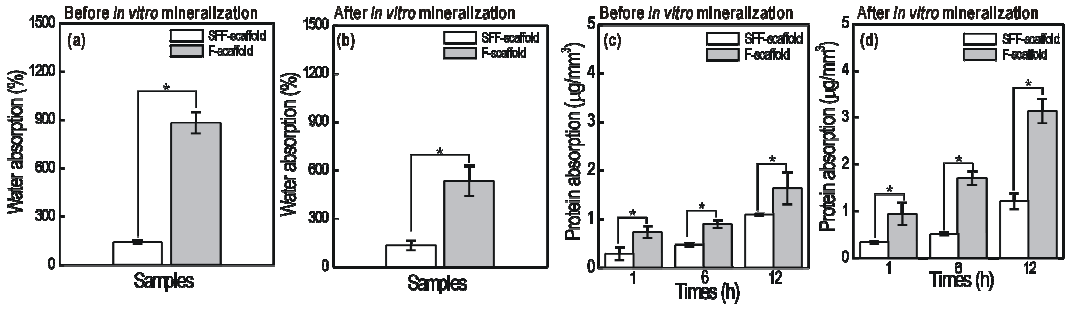

Figure 6. The ability of water absorption for F-scaffold and SFF-scaffold (a) before and (b) after *in vitro* mineralization. Protein absorption on F-scaffold and SFF-scaffold (c) before and (d) after *in vitro* mineralization after 1, 6, and 12 h.

RSC Advances Accepted Manuscript

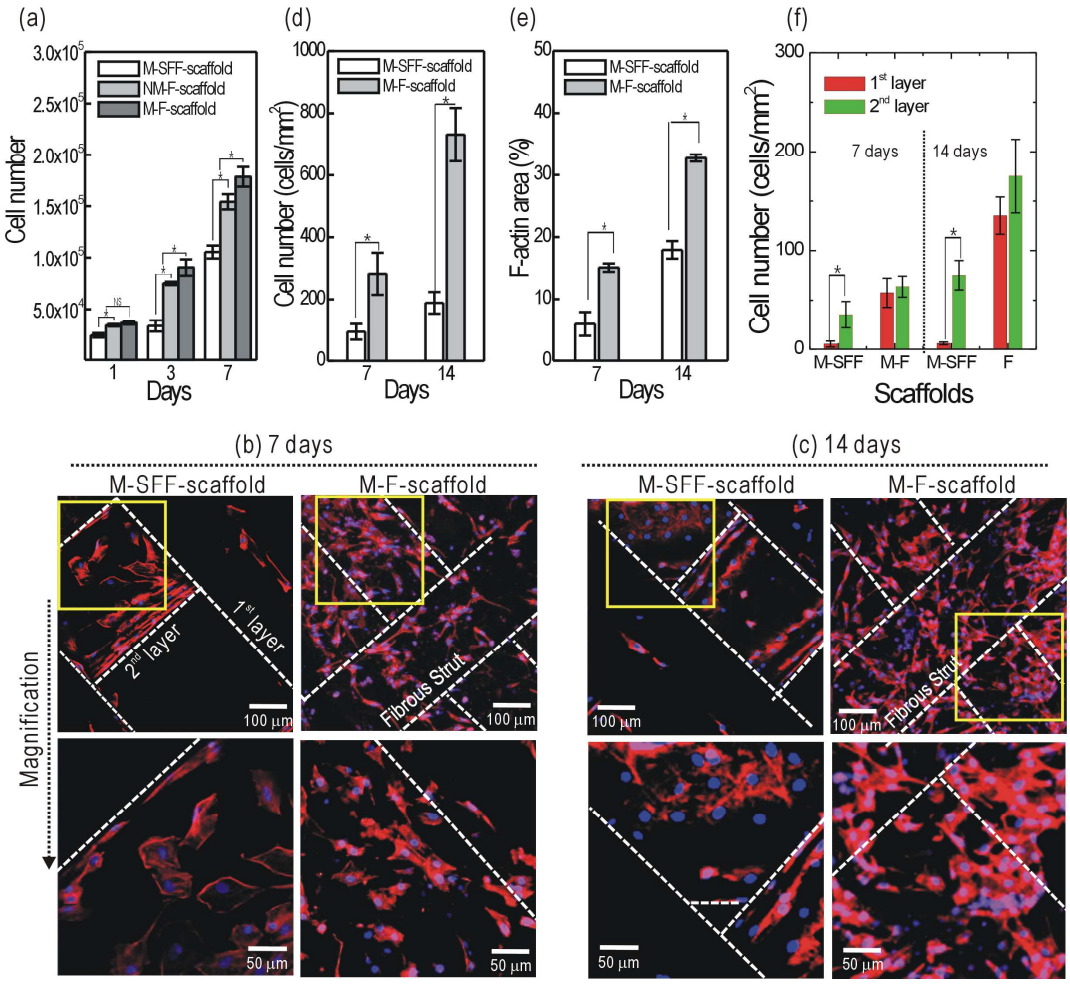

Figure 7. (a) MC3T3-E1 cell proliferation (optical density) at 1, 3, and 7 days, as determined by MTT assay on M-SFF- and M-F-scaffolds. DAPI/phalloidin images of M-SFF and M-F-scaffolds after culture for (b) 7 and (c) 14 days. (d) The number of nuclei and (e) F-actin areas after culture for 7 and 14 days. Data are means ± standard deviations. (f) Cell numbers on first and second and layer struts after 7 and 14 days. Asterisks indicate significant differences.

RSC Advances Accepted Manuscript

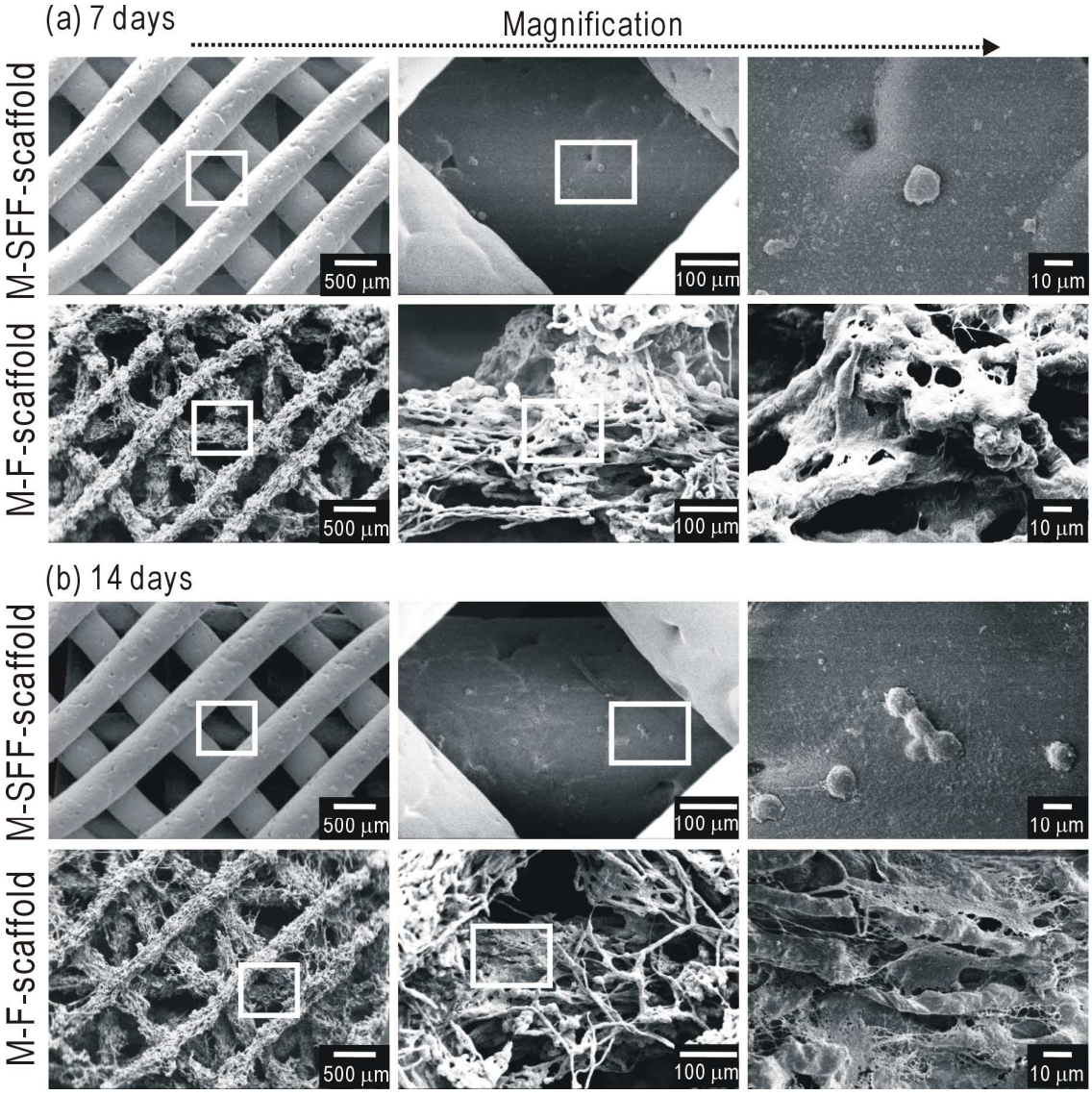

Figure 8. Scanning electron micrographs of M-SFF and M-F-scaffolds after culture for (a) 7 and (b) 14 days.

RSC Advances Accepted Manuscript

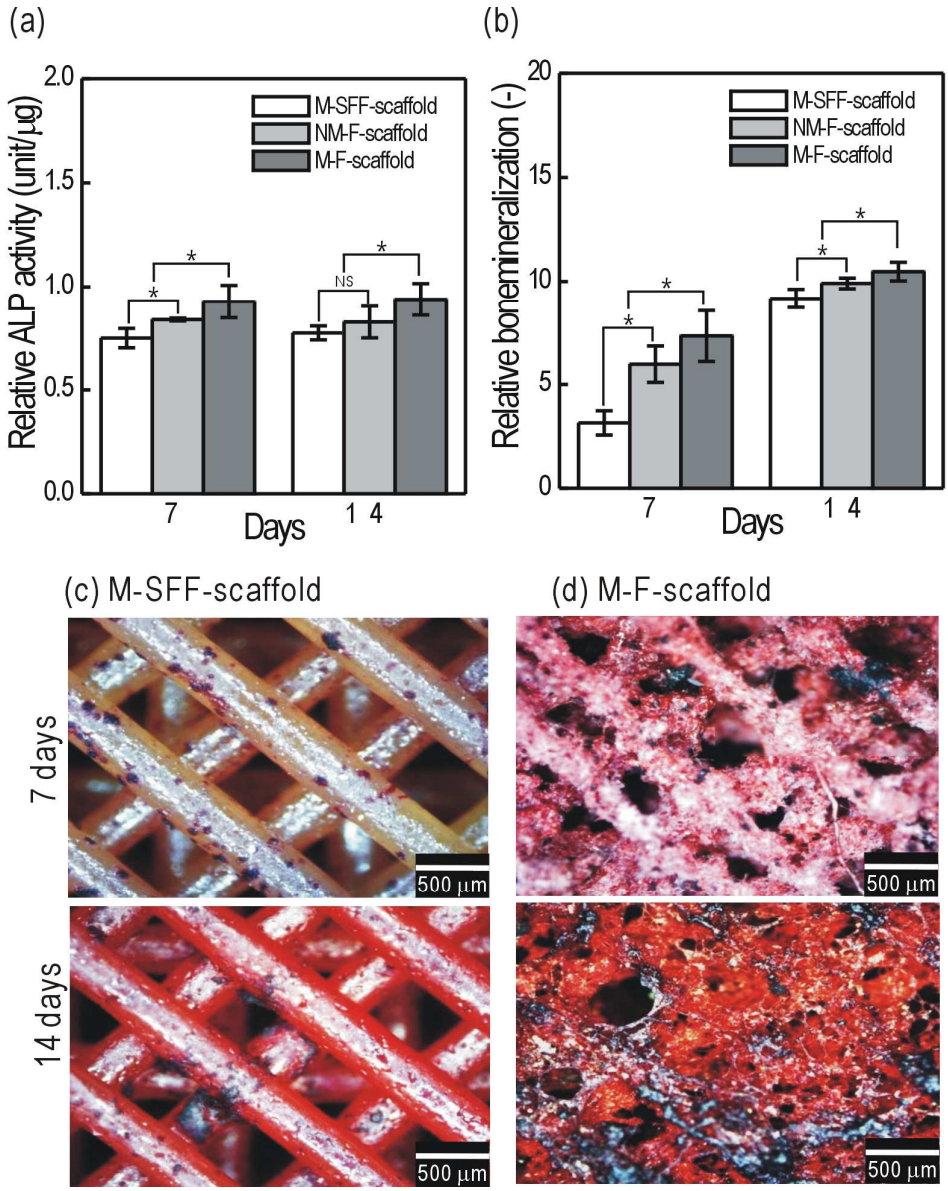

Figure 9. (a) Alkaline phosphatase (ALP) activities and (b) calcium mineralization by MC3T3-E1 cells in M-SFF, NM-F, and M-F-scaffolds. Optical micrographs of ARS staining of the (c) M-SFF-scaffold, and (d) M-F-scaffold after 7 and 14 days of cell culture.

RSC Advances Accepted Manuscript